Final Report for the OTKA Project K-116516

Peter Galajda

Our project primarily aims to explore the connections between cellular aging, cell-to-cell variability, and their effect on microbial life. The following four goals were defined in the original proposal, which we addressed as described below.

1. *Development of an experimental setup based on optical micromanipulation and microfluidics.*
We constructed several single-cell traps for bacteria and algae and we applied them for single-cell and population-level studies on aging and maturation.

2. *Measuring cell cycle parameters in the context of cell lineage relationships and cell pole age.*
We measured cell cycle length, the timing of divisions, and cell length at division for *Pseudomonas aeruginosa* (during quorum sensing) and *Escherichia coli* cells (with and without antibiotic stress).

3. *Measuring physiological parameters and flagellar activity in the context of cell lineage relationships and cell pole age.*
We measured the linear elongation rate for *P. aeruginosa* (during quorum sensing) and *E. coli* cells (with and without antibiotic stress). We analyzed membrane permeability/cell integrity using fluorescent staining in *E. coli* in antibiotic stress. We are working with Gaszton Vizsnyiczai (OTKA project id. 138520) on the precise characterization of flagellar activity.

4. *Measuring noise in gene expression patterns in the context of cell lineage relationships and cell pole age.*
We measured gene expression levels under quorum control in *P. aeruginosa* cells and compared mother cells (with the oldest poles) to other cells.

We applied the acquired cell trapping experience to collaborate on single-cell level phenotypic characterization of algal cells. We extended our research scope beyond cell level aging to also analyze population/community level maturation (phenotypic and genetic heterogeneity).

Development of microfluidic cell traps to track and control cell lineages

We evaluated two strategies for the realization of prolonged trapping of bacterial cells. Optical trapping-based solutions proved to be unpractical for several reasons. First, we did not manage directly trap bacterial cells with laser tweezers for extended periods of time without severely affecting their physiological state (reflected by their flagellar motility and growth). Applying oxygen scavenging systems and anaerobic conditions to reduce damage due to reactive oxygen species yielded only partial success. To avoid the direct interaction of bacteria with intense laser beams we tried to attach microbeads to cells as optical "handles" that can be grabbed by the laser beam. In this case cell attachment to the beads proved incidental, often beads attached to the side of the cell instead of the ideal pole attachment. Stable trapping of cells in nutrient medium flow also proved to be difficult, with a heavy compromise between trapping force and the number of cells trapped. Therefore early in the project, we decided to focus on the development of microfluidic cell traps that can stably grab large numbers of single cells. Two types of microfluidic devices are
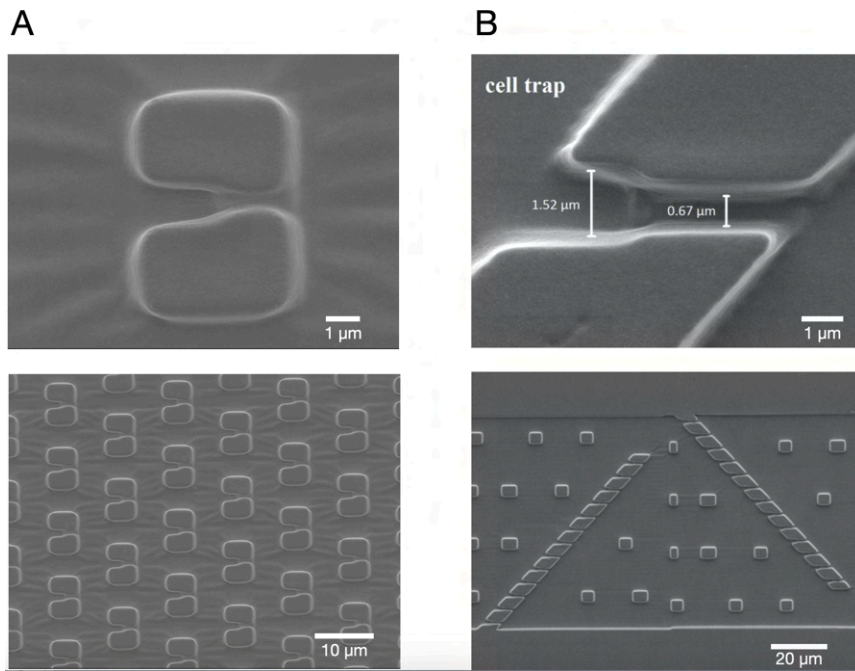
Figure 1. Scanning electron micrographs of microfabricated traps for bacterial cell trapping. A) individual cell traps. B) Cell traps along a zigzag pattern to trap cell progeny (baby machine).

shown in Fig. 1. The device in Fig. 1A consists of an array of individual single-cell traps in a channel. The traps of the device shown in Fig. 1B (which we named the "baby machine") are arranged along with a zigzag pattern within a channel. This second device is designed so that
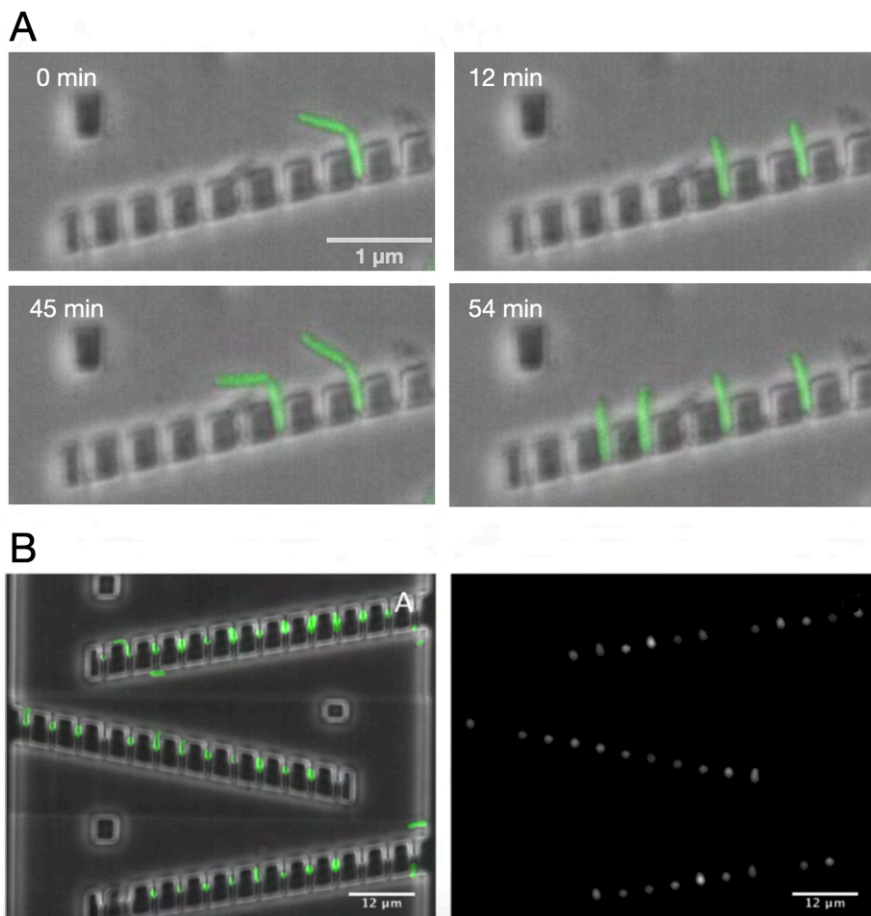
Figure 2. Baby machine with trapped *E. coli* bacteria. A) frames from a time-lapse recording of cell division and progeny trapping (composite images of phase contrast and fluorescence microscopy images). B) Traps filled up with cells (left: composite image, right: fluorescence image).

following cell division, one of the daughter cells remains in the original trap while the other one is carried into the next free trap by the fluid flow (Fig. 2A). This "automated trapping of progeny" offers great advantages and possibilities compared to the device in Fig. 1A. By utilizing an optical tweezer the first trap in the zigzag array can be populated by a single founder cell. Following subsequent divisions, the progeny of the founder cell remains in the device until all the traps are filled (Fig. 2B). Up to this point, the full lineage tree can be traced, while a partial lineage tree may be further investigated after the complete filling of the device. At any time optical tweezers may be used to remove cells from the traps, with the possibility of grabbing later progeny cells in these traps to control the traced branches of the lineage tree. Furthermore, since the orientation of rod-shaped bacterial cells is fixed by the geometry of the trap, cell poles may be tracked to analyze any effects related to cell pole aging (Stewart 2005). We proved the usability of the device by trapping *E. coli* cells for tens of generations, with optical tweezers control over the tracked branches of the lineage tree. We are preparing the manuscript from these results [Ábrahám 2022a].

Single-cell level phenotypic studies

Quorum sensing in confined *P. aeruginosa* cells

Quorum sensing is a mechanism to achieve cell density-dependent gene regulation in bacteria by means of excretion and sensing of small signaling molecules. Although most often thought of as a population-level phenomenon, the importance of single-cell level studies is getting widely recognized [Striednig 2021].

We applied a microfluidic mother machine [Wang 2010] to study the single-cell level quorum sensing response of *P. aeruginosa* in periodic waves of signal molecules to explore the role of phenotypic heterogeneity and aging in quorum sensing. Instead of applying static conditions, fluctuations in signal molecule levels were used to potentially amplify the effects of cell-to-cell variations in physiological state, metabolic activity, and gene expression levels, among others.

In this work [Ábrahám 2022b], we tracked cell lineage information, cell division, cell size, and quorum-controlled GFP expression in *lasI*-deficient *P. aeruginosa* PUPa3 cells by fluorescence time-lapse microscopy. This strain is not able to synthesize the signal molecule N-3-Oxo-Dodecanoyl-L-Homoserine Lactone (C12-HSL), but it is sensitive to it. Furthermore, in this particular strain, the feedback between the Las and Rhl quorum signaling circuits is broken, which ensures that the response of the Las system depends solely on C12-HSL. The application of a reporter plasmid (containing a GFP(ASV) gene behind a quorum-dependent promoter) offers a simple way to follow the quorum state of the cells by means of fluorescence microscopy.

Cells were seeded in the narrow side channels of the device by wetting or using optical tweezers (Fig. 3A). Here dividing cells form a chain, and cells gradually get pushed out of the side channel and carried away by the flow in the main channel (Fig. 3A-B). Nutrient medium with and without C12-HSL signal molecule was flown in the main channel from which signal molecules diffuse into the side channels where bacteria reside. Our numerical simulations show that the concentration of C12-HSL (and other small molecules) in the side channel equilibrates with the concentration in the main channel within 2 s.

Altogether 10,766 cells were analyzed during the 65-hour time course of the experiment. The average fluorescence intensity of cells changed in accordance with the presence of the signal molecules (Fig. 3B-C, Fig. 4A). Upon exposure to high C12-HSL concentration, the fluorescence intensities increased in time and started to level off in around 6 hours. Withdrawal of the signal molecules resulted in the decrease of the fluorescence signal. This cycle repeated with
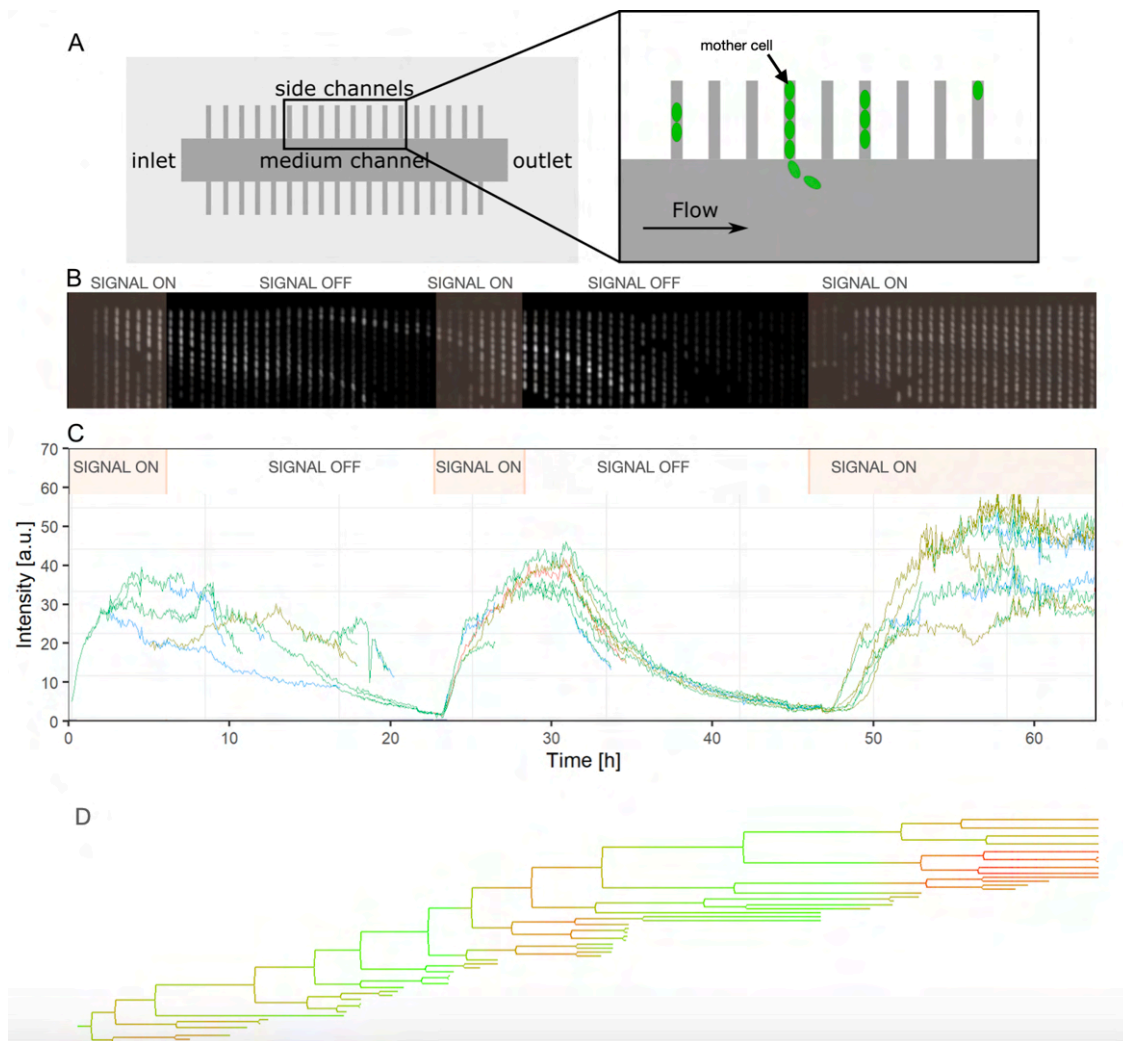
Figure 3. Single cell quorum sensing experiments on *P. aeruginosa* using a mother machine. A) Schematic drawing of the microfluidic device (not to scale), the inset shows the cells in the side channels. B) Kymograph of fluorescent micrographs of cells in a particular side channel (see the time axis on panel C; the ping color offset represent the presence of the signal molecules). C) Fluorescence intensity vs. time in a particular side channel. Each line show data corresponding to a single cell. Branching of lines represent cell divisions, end of lines represent cells dropping out of the side channel. D) Cell lineage tree constructed for the same cells that were analyzed in panel C. The color of the branches represent the fluorescence intensity of cells (green-low, red-high).

approximately the same kinetics, although a slight drift towards higher intensities was observed. There was a considerable variation of the intensities on the single-cell level. Since the population average of the intensity fluctuates in time, the coefficient of variation (CV in short; it is the ratio of the standard deviation and the mean) characterizes the heterogeneity of the population better than the standard deviation. Fig. 4B shows the population-wide CV in time for the cellular intensities. CV changed in synchrony with the presence of C12-HSL and the quorum state of the cells, and it was the lowest in the presence of C12-HSL or in the quorum-sensing-on state. The dynamics, however, were markedly different in the case of the C12-HSL on->off and off->on transitions. CF dropped abruptly (on the timescale of about 1 h), and without a delay for C12-HSL off->on transition. On the other hand, there was a considerable, 2 h long lag time for C12-HSL on->off transition which is followed by a gradual, seemingly linear increase in CF. This tells us that when comparing the relative cellular intensities within the population there is a higher level of heterogeneity in the late phase of the exit from the quorum-sensing-on state.

The average cell size right before division (and the average cell size) was relatively uniform in time, only showing about ±5% fluctuation during the signal on-off cycles (Fig. 5A-B).
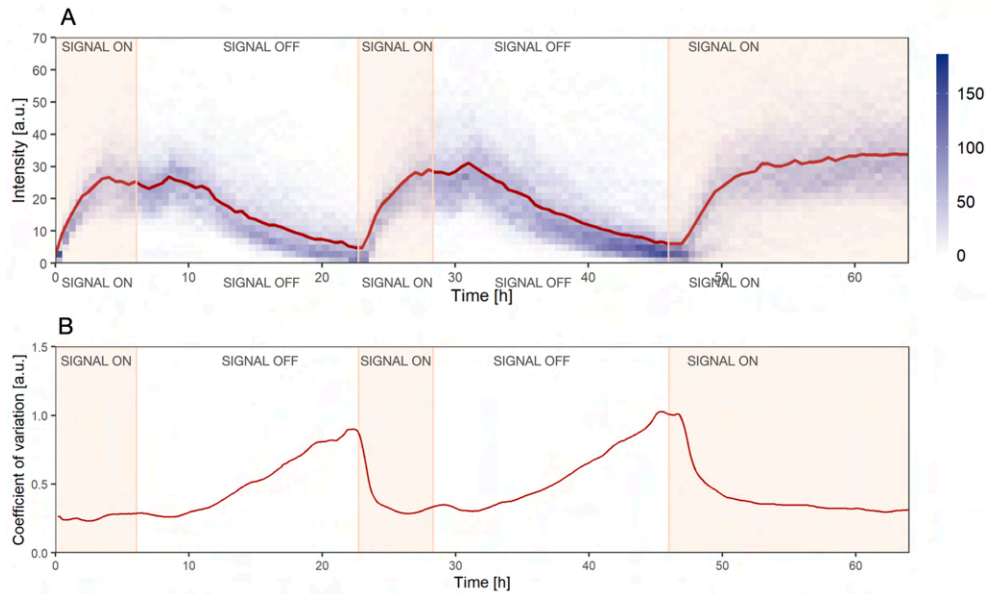
Figure 4. Population level statistics of single cell fluorescence intensity data. A) Red line - population average of fluorescence intensity vs. time. Shades of blue represent the number of cells with a particular (binned) fluorescence intensity at a defined time (see colorbar). B) Coefficient of variation of single cell fluorescence intensities vs. time.
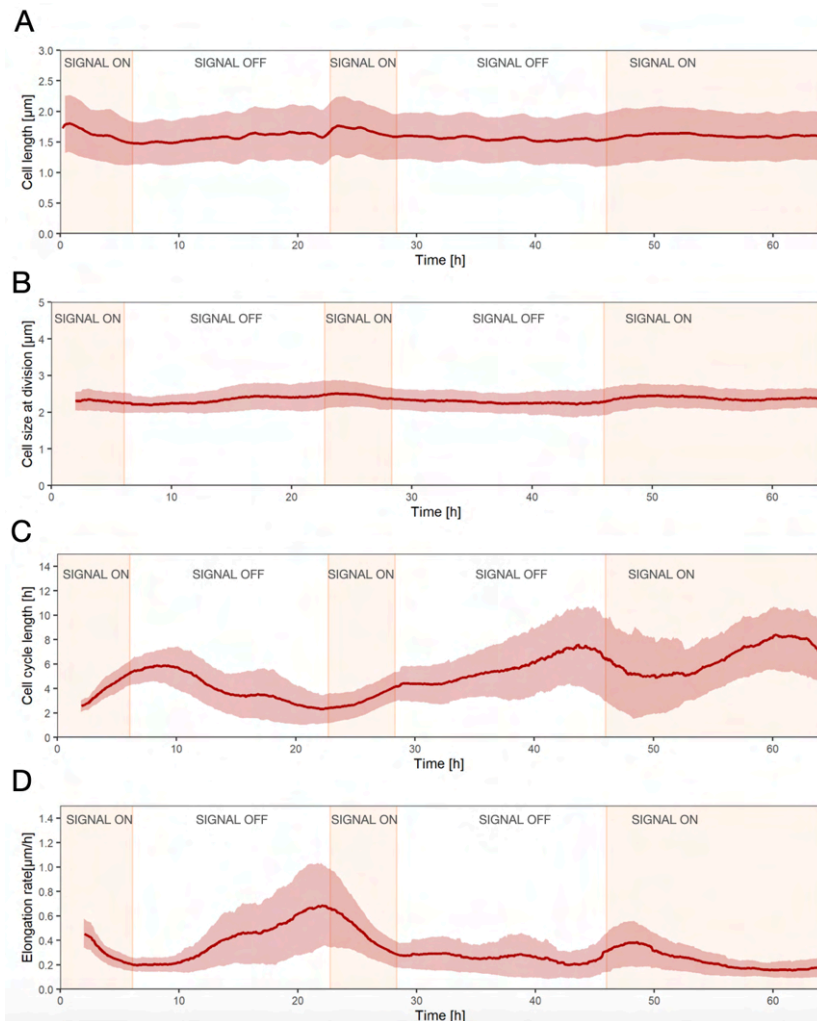
Figure 5. Population level statistics of single cell phenotypic characteristics.. Dark red lines represent population averages, the red bands represent the standard deviation. A) Cell length in time. B) Cell length right before division in time. C) Cell cycle length in time (the midpoint of the cell cycle is the assigned time here). D) Linear cell elongation rate in time.

5

Consequently, the average cell length right after cell division was similarly unvarying (data not shown). This demonstrates that the cell size is under tight regulation that is not affected by quorum sensing.

The average cell cycle length (measured as the time elapsed between divisions), on the other hand, changed more during the time course of the experiment (Fig. 5C). Although it didn't show a clear regular periodicity along with the signal on-off cycles, some characteristic features may be identified. The cell cycle length tends to increase during all signal-on periods. A decreasing trend is observed in the first signal-off period, while it climbs in the second one. Next, we looked at the linear cell elongation rate, defined as the difference between cell length measured at the beginning and end of the cell cycle, divided by the cell cycle length. The elongation rate demonstrates an anti-phase fluctuation with respect to the cell cycle length, as shown in Fig. 5D. This doesn't come as a surprise considering the quasi-uniform nature of the cell size before (and after) division. Hence the fluctuation of the elongation rate is largely determined by the reciprocal cell cycle length.
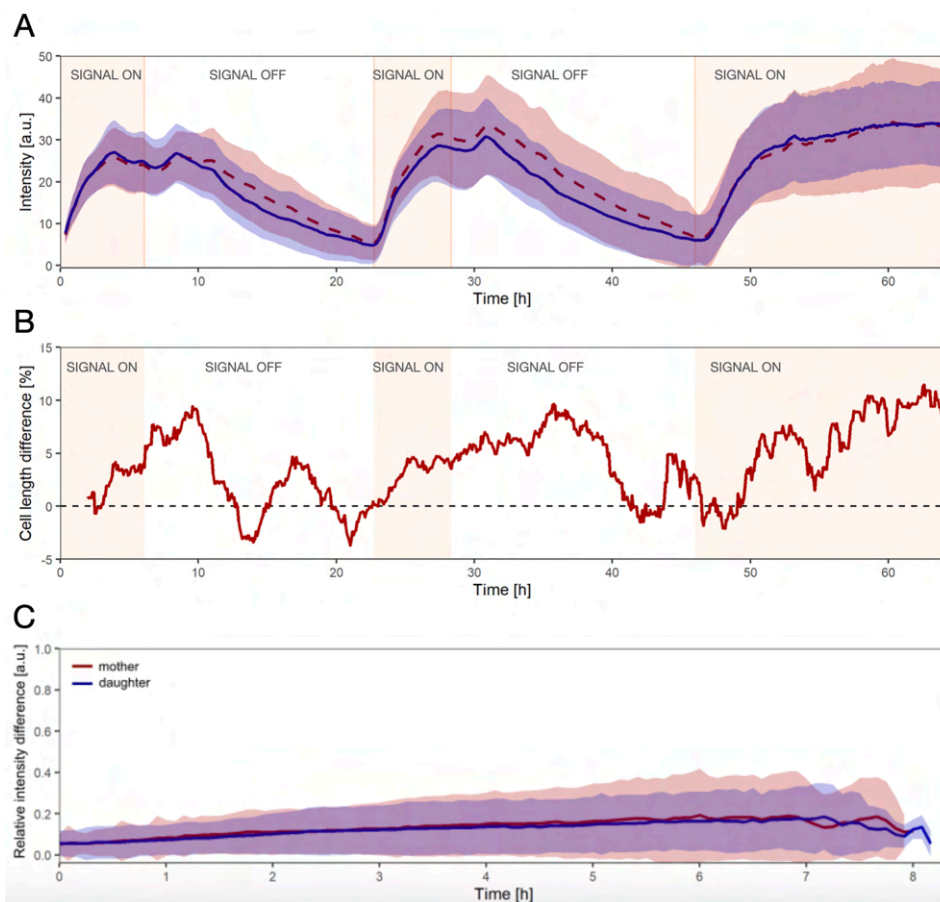
Figure 6. Comparison of various phenotypic parameters between mother cells and non-mother cells. A) Average fluorescence intensities. Red dashed line: average of mother cells. Blue line: average of non-mother cells. Light red and blue bands: corresponding standard deviations. B) cell length difference between non-mother cells and mother cells

Due to the construction of the microfluidic mother machine, some cell lineage information can be tracked during the experiments. We refer to the cells deepest in the narrow, dead-end side channels of the device as the mother cell (as in [Wang 2010]). The pole of the mother cell that falls towards the dead-end of the channel is the old pole, which is inherited from one generation to the next. The other pole is newly constructed in each generation. The aging old pole makes the mother cell special compared to all the other cells in the device. We tracked 68 mother cells and their progeny in the device, for which we were able to construct cell lineage trees (Fig. 3D)

Fig 6A shows the average fluorescence intensity of the mother cells as well as the average intensity of all other cells. The difference seems to be marginal in the signal-on periods, while in the signal-off periods a somewhat faster fall in intensity is observed for the mother cells. The cell length right before the division is smaller (Fig. 6B), while the cell cycle seems to be somewhat longer for the mother cells (data not shown).

In order to gain some insight into the emergence of cell-to-cell heterogeneity of the fluorescence intensity, we traced the normalized intensity difference between daughter cells during the period of a single cell cycle. Interestingly we found a linear increase in the relative intensity difference in time (Fig. 6D). We divided the cells into two groups. The quorum-on state was assigned to those cells with an average intensity over 18 a.u., and cells with an intensity below this threshold were labeled as quorum-off. There is a slight difference between these two groups of cells in terms of the normalized intensity difference between the daughters (data not shown). There seems to be a slightly larger difference between the daughter of quorum-on cells. This explains the previous observation about the higher CF values (i.e. a higher level of heterogeneity) in the cell level intensity data (Fig. 4B). We also analyzed the intensity difference for mother and non-mother cells. We found that although the average intensity difference seems to be the same for these two groups, mother cells demonstrate move variability (Fig. 6D).

We were able to construct cell lineage trees originating from all 68 mother cells (see Fig. 3D as an example). These trees are asymmetric and partial due to the continuous dropout of cells from the side channels. Still, analysis of phenotypic traits in light of cell lineage information was possible. Here we define cell lineage distance (CLD) as the total number of cell divisions separating cells from their lowest common ancestor [Zhao 2021]. CLD is 2 between pairs of daughter cells, 4 between cousins, etc. CLD is always an even number between pairs of cells from the same generation, while it may be an odd number when comparing cells from distinct generations. We analyzed the normalized fluorescence intensity difference of pairs of cells concurrently present in the device, as a function of their lineage distance (Fig. 7).
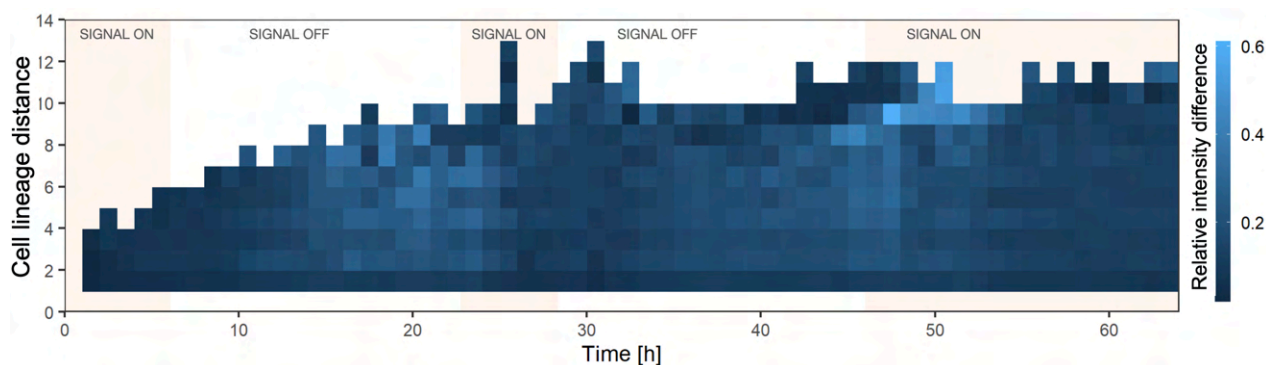
Figure 7. Relative intensity difference as a function of time and cell lineage distance. Data are binned in time in 1 h intervals.

Data show that the standard deviation of the intensity difference is below XX at all CLD in population-level quorum-off states (i.e., when the population average of fluorescence intensity is below the threshold 18). The standard deviation is higher in the quorum-on state and increases for higher CLD values. This analysis demonstrates the power of cell trapping based microfluidic methods to perform detailed phenotypic analysis in combination with precise cell lineage tracking.

Studying algal cells using microfluidic cell traps

During the project decided to exploit the experience in microfluidic cell trapping we gained during the project may be readily applied to study phenotypic heterogeneity, the cell cycle, and in connection with these, aging in other cell types. This lead us to collaborations with the research

groups led by Imre Vass and Szilvia Z. Tóth (Biological research Centre, Szeged) to develop and apply microfluidic cell traps to study algal cells.

Chlamydomonas reinhardtii is a model organism of increasing biotechnological importance, yet, the evaluation of its life cycle processes and photosynthesis on a single-cell level is largely unresolved. To facilitate the study of the relationship between morphology and photochemistry, we established a microfluidics-based platform in combination with chlorophyll a fluorescence induction measurements [Széles 2022]. Together with the collaborators we designed, constructed, and employed two types of microfluidic devices for single-cell analysis of *C. reinhardtii*. In addition to morphological examinations by microscopy, chlorophyll a fluorescence induction measurements were also conducted, thus a complex physiological assessment of *C. reinhardtii* cells trapped in microfluidic devices became possible. Two main device types were developed: the traps of the "Tulip" device (Fig. 3) are suitable for capturing and immobilizing individual cells enabling the measurement of their photosynthetic activity. The traps of the "Pot" device (Fig. 8) capture single mother cells and enable cell divisions while retaining the daughter cells.

The aim of constructing the "Tulip" microfluidic device was to trap and immobilize individual cells enabling high-quality chlorophyll a fluorescence measurements. The dimensions of the traps were optimized for stable trapping (Fig. 8B) and limiting cell movement for high precision fluorescence measurements (Fig. 8C). Non-photochemical quenching (NPQ) measurements were carried out on an ascorbate-deficient mutant (Crvtc2-1) and wild-type (CC-4583) cells in various growth media and light intensities. As shown in Fig. 8D, NPQ of the Crvtc2-1 mutant was about twice as high as in the wild-type when grown under photoautotrophic conditions. NPQ relaxation of the photoautotrophic cultures was rapid. The "Tulip" platform could be particularly useful to study (1) population heterogeneity upon various treatments and (2) the effects of inhibitors, pollutants, and other compounds on the morphology and photosynthesis of *C. reinhardtii*. Evidently, not only NPQ but other parameters could be traced and related to cell age.
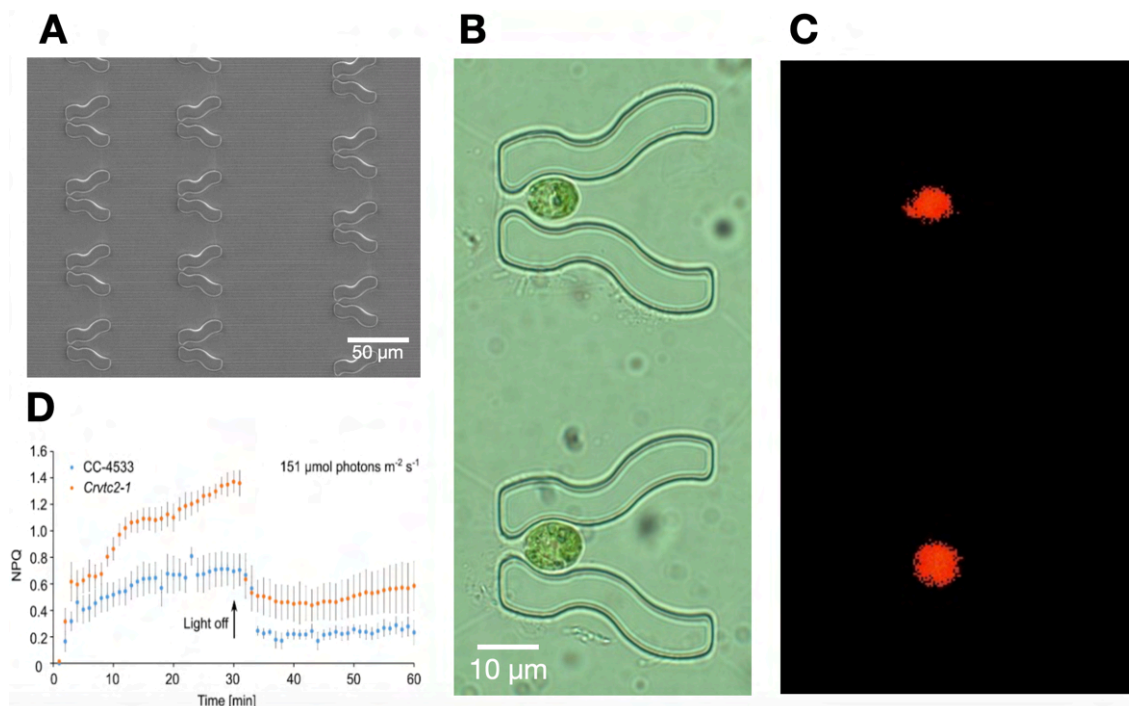
Figure 8. "Tulip" trap for algal cells. A) Scanning electron micrograph of a trap array. B) Brightfield microscopy image of *C. reinhardtii* cells in the traps. C) Fluorescence microscopy image of the cells shown on panel B (chlorophyll a fluorescence). D) NPQ in time measured on trapped single cells (Crvtc2-1 and CC-4583 strains).

In order to capture and retain the mother cells and the daughter cells within the same traps we designed seven types of so-called "Pot" traps, arranged in arrays within parallel channels in a microfluidic device (Figure 9). These traps differed in the inlet geometry (both on the inner and outer side of the trap entrance) and the number of outlet slits. We developed a novel method to construct the device of two layers to keep the width and depth of the slits low enough (about 3 and 4 μm, respectively) to retain the smaller daughter cells while ensuring a larger depth (12 μm) of the trap itself to accommodate the mother cells without much physical constraint. Cell cycle was monitored in cells originating from synchronized cultures grown in light-dark cycles, for 48 h. After loading the device, cells started to grow in size. In parallel, their F_V/F_M (variable chlorophyll fluorescence divided by maximum chlorophyll fluorescence) value decreased 8 h after loading (Figure 9B). Cell division occurred at around 24 h, and the daughter cells remained inside the traps —their F_V/F_M values were relatively high (about 0.51). These data demonstrate that the cell cycle of *C. reinhardtii* is accompanied by changes in photosynthetic efficiency. Using the "Pot" microfluidics platform, we demonstrated that photosynthetic efficiency changes during the cell cycle. This raises the possibility that the photosynthetic apparatus undergoes some sort of remodeling upon cell and chloroplast division.
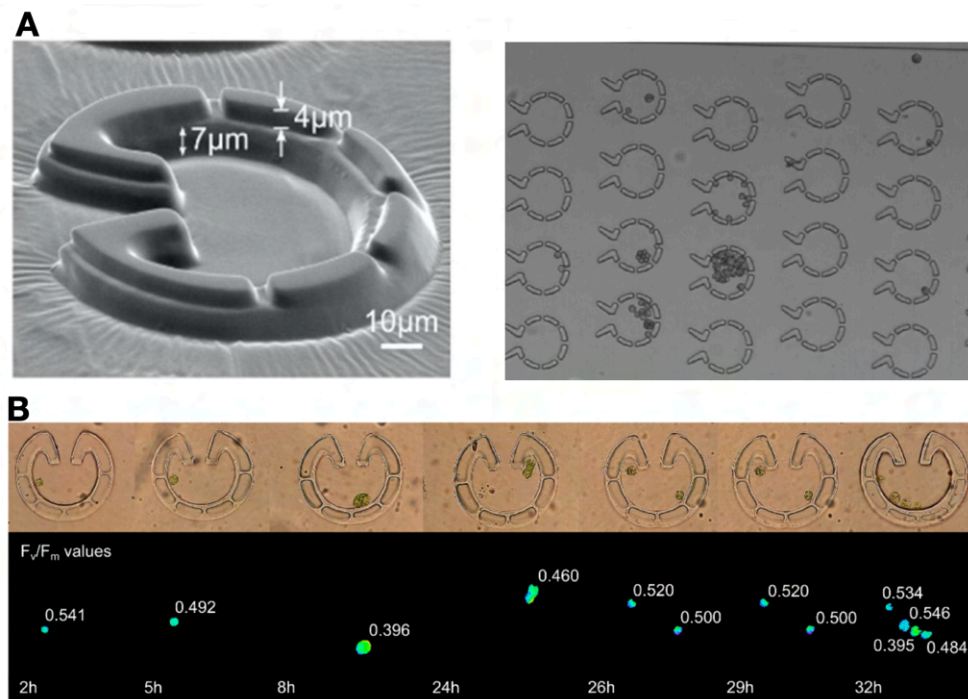
Figure 9. "Pot" trap for algal cells. A) Left: scanning electron micrograph of a trap. Right: brightfield microscopy image of *C. reinhardtii* cells in the traps. B) Time lapse series of brigtfield images of cells in a trap, and the corresponding spatial F_V/F_M values.

Symbiodinium spp. are the crucial symbiotic component of reef-building corals and a primary producer in the aquatic ecosystem on Earth. We investigated the morphological differences and the the cell division pattern in intact *Symbiodinium* cells and protoplasts [Bashir 2022].

The microfluidic system was designed to trap cells and keep them in precisely controlled environmental conditions, considering medium, temperature, and flow rate (Fig. 10A). Individual cells were captured in the traps, which allowed the characterization of the morphological and physiological changes of single cells throughout the experiments. An enzymatic cell wall digestion and regeneration protocol was used for *in situ* formation of protoplast from trapped cells, and recreate the cell walls and the normal cell morphology in a later phase.

The cells were in the dividing phase (Fig. 10B) and motile forms in the device before enzyme treatment, but after 1 hour of enzyme treatment most of the cells stopped moving and cell division also halted. However, some of the cells still divided in the protoplast phase. Interestingly, protoplasts divided into two rounded non-motile daughter cells (Fig.10C), as opposed to the cell division of non-digested control cells, where two spindle-shaped motile daughter cells are formed. The cell division pattern was different after regeneration of the cell wall as compared to
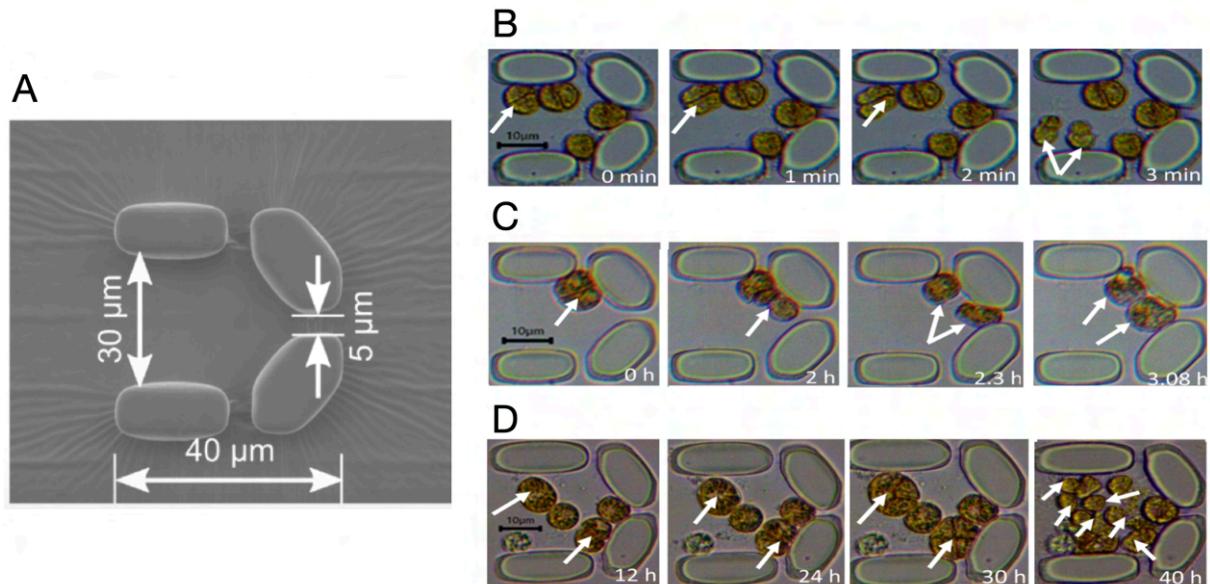
Figure 10. Traps for Symbiodinium spp. cells. A) Scanning electron micrograph of a trap with the characteristic dimensions indicated. B)-D) Time-lapse microscopy images of cell divisions. B) untreated cells. C) Protoplasts. D) Recovered cells.

untreated cells. In normal cell division, the mother cell divides into 2 or 4 daughter cells (Fig. 10B), but after regeneration, more than 4 daughter cells were formed with maximum division into 8 daughter cells with cell sizes smaller than normal daughter cells (Fig. 10C). In intact cells, the division process into 2 motile daughter cells was completed in 3 minutes, whereas in the protoplast stage the division process required 3 hours to complete and it resulted in two round and non-motile cells instead of motile and spindle-shaped daughter cells. These daughter cells expanded in size after cell division. These results indicate that *Symbiodinium* cells that are undergoing cell wall digestion are able to divide (albeit with low efficiency), and the daughter cells formed during the cell wall digestion procedure are prone to protoplast formation with higher efficiency than non-dividing cells.

Maturing populations: heterogeneities in bacterial communities in confined spaces

Maturation, a concept analog to aging, has been applied to ecosystems for several decades [Odum 1969]. Lately, it has been used more and more in the context of microbial communities [Beller 2021]. Due to the similarity between the concepts of aging and maturation, we expanded the scope of our work to study the aging/maturation/development of bacterial populations and communities, with a focus on the role of environmental heterogeneities. For this, microfluidics proved to be an indispensable technology [Nagy 2018, Wetherington 2021]. In light of our results in this area, we

are actively working on establishing a strong connection between cellular aging and population-level maturation.

The emergence of resistant bacteria in antibiotic and phage gradients

We aimed to explore how different forms of heterogeneities (and their change in time) affect the susceptibility of bacteria to antibiotics and the evolution of resistance. On one hand, in an ongoing work we are exploring the cell-to-cell variation of antibiotic susceptibility in microfluidic baby machine and mother machine devices (Fig. 11). Currently, we are finalizing data analysis collected in experiments and preparing for writing a manuscript. We explored the heterogeneous timing of cell death (membrane permeabilization demonstrated by fluorescent dyes), and we were not able to demonstrate any effect of the cell pole age.
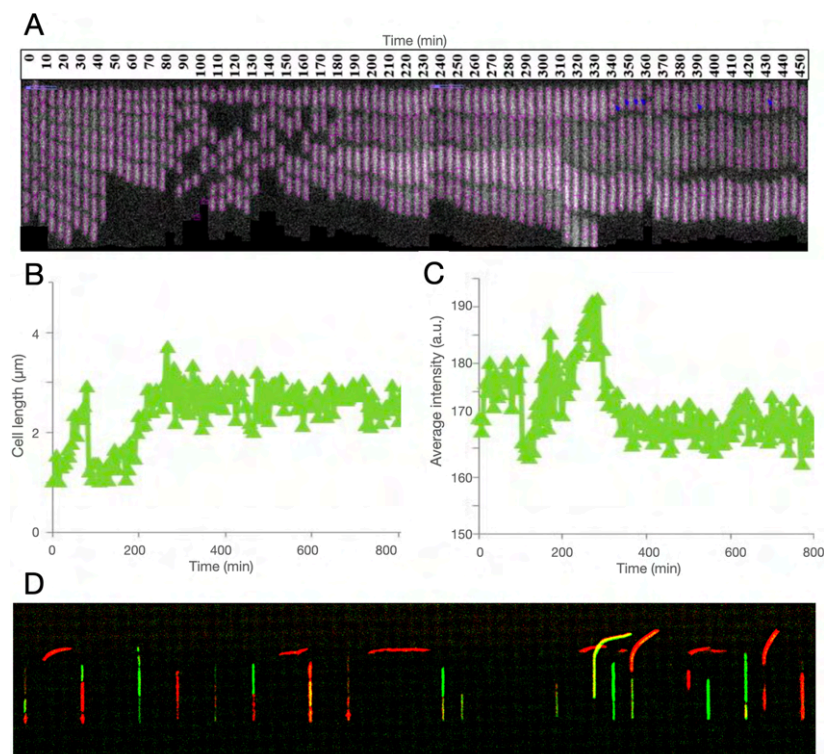
Figure 11. Treatment of *E. coli* cells with ciprofloxacin in the mother machine. A) Kymograph of fluorescence microscopy images of GFP expressing cells in a side channel. B) Cell length of the mother cell of panel A in time. C) Average fluorescence intensity of the mother cell of panel A in time. D) Fluorescence microscopy image of ciprofloxacin treated cells in the mother machine after live/dead staining (green-live, red-dead).

In population-level studies, we applied a microfluidic gradient generator device (Fig. 12A) to study the emergence of resistant bacteria in spatial antibiotic gradients [Nagy 2022a]. The left reservoir of the device was filled with culture medium containing high (3-6× minimal inhibitory concentration, MIC) concentration of ciprofloxacin. The right reservoir was filled with antibiotic-free medium. A linear spatial concentration gradient formed in the central observation channel due to the diffusion of ciprofloxacin between the reservoirs. The observation channel was inoculated with a nonresistant GFP expressing *E. coli* culture (MIC of 16 ng/ml).

After inoculation cell growth was limited at the higher antibiotic concentration on the left side of the channel. Concurrently with this growth inhibition, we observed the formation of biofilm-like dense cell assemblages that localize in the region with sublethal antibiotic dose on the right and from which a sharp frontline population starts expanding to the left across the width of the channel (Fig. 12B). Microscopy images show a quasi-static texture over these biofilms, suggesting the

dominance of sessile cells within these structures. We often saw streams of bacteria with varying levels of brightness, which is considered as a sign of radiating phenotypic diversity on display. The streams are formed by fast-growing subpopulations which emerge at specific locations on the low ciprofloxacin (right) side of the observation channel and later spread across it at a higher rate than the surrounding cells This intense colonization started within the first 10 hours of the experiments. MIC measurements on extracted bacteria show a mild (~2×) increase in MIC in samples exposed to the antibiotic gradient for 48 h. This suggests that this early expansion is rather due to the protective function of the biofilm as high resistance mutations only appear after the late phase of the experiment when up to 30× increase in MIC was measured. MIC change correlates with the duration of exposure to the antibiotic gradient. Samples extracted after 48 hours typically exhibit a 2-4×MIC change, while a 1-30× change was measured for samples collected after 72 hours. MIC values vary even within samples taken from a single experiment, which demonstrates a compound community development and maturation in the microfluidic habitat, giving rise to genetic diversity. A biofilm assay revealed a diversity of biofilm-forming ability for the isolated mutants
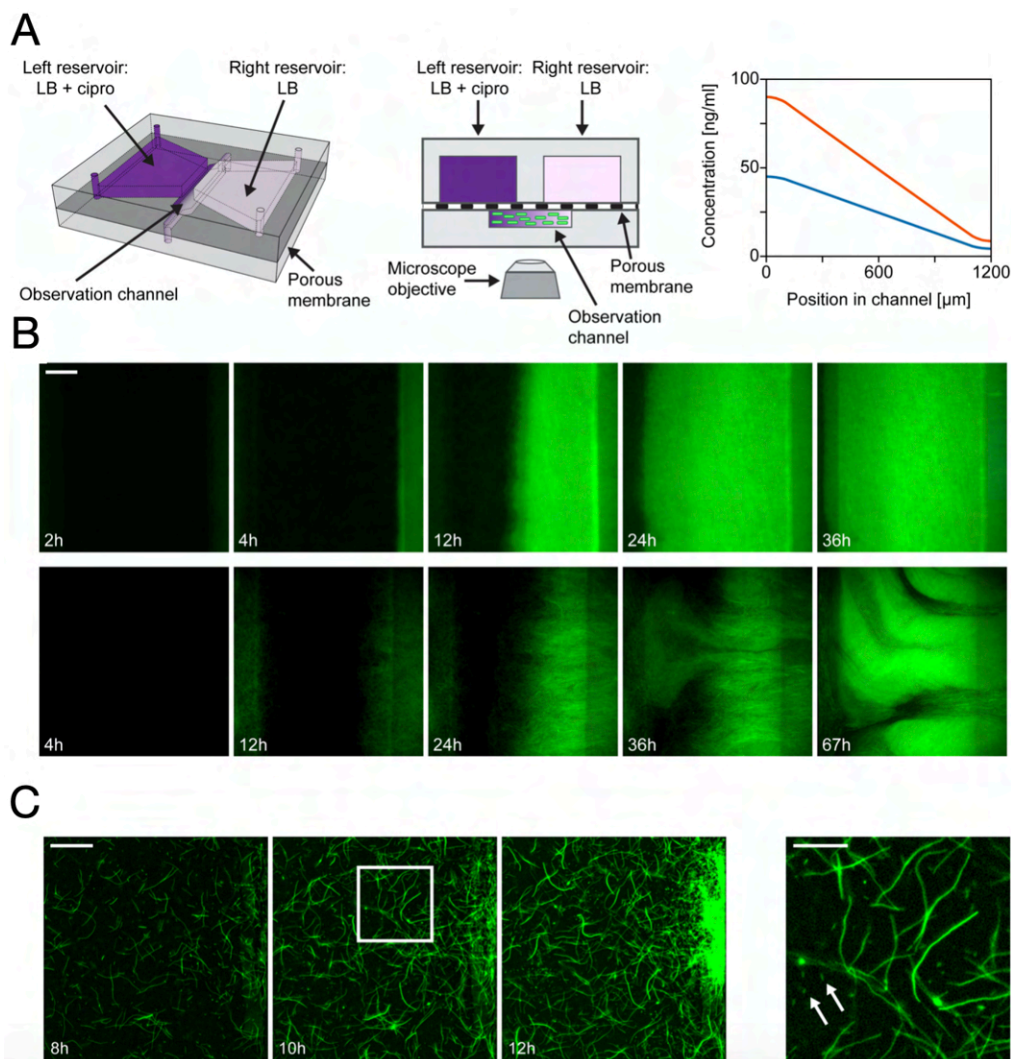
Figure 12. *E. coli* in ciprofloxacin gradients. A) Schematics of the gradient generator microfluidic device in (left) perspective and (middle) cross-sectional view. Right: calculated ciprofloxacin concentration across the observation channel in case of 96 ng/ml (6×MIC, orange) and 48 ng/ml (3×MIC, blue) maximal concentrations. B) Time-lapse fluorescence microscopy images of a propagating biofilm front in a 3×MIC ciprofloxacin gradient. The scale bar is 200 μm. C) Emergence and growth of a resistant subpopulation on the low antibiotic concentration side of the observation channel. Series of fluorescence images taken at different time points of the experiment (scale bar is 50 μm). Right: zoom-in of the image taken at 10 h to show *E. coli* cells with different morphologies (scale bar is 20 μm). Arrows indicate some normal size rod-shaped cells among filamentous ones.

We analyzed cell morphology in gradients with 3×MIC maximal ciprofloxacin concentration. We found that most cells exhibit an elongated, filamentous shape in response to ciprofloxacin; there are, however, some bacteria with normal rod-shaped morphology as well (shown by arrows in Figure 12C). Although these filamentous cells show less surface attachment and mobility, they formed a dense intertwined multicellular mass that maintained some spatial structure.

Compartments with different levels of antibiotics (patchiness) may harbor various mutants with various degrees of resistance at the landscape level. Subsequent mutations, occurring first within local populations living in regions with lower antibiotic concentrations, increase the resistance level and may expand into other antibiotic-rich compartments. This is in accordance with the concept of *selection amplifiers* [Tkadlec et al., 2021], structures in which antibiotic-resistant variants enrich. Although our microfluidic device is spatially distributed, it lacks such an explicit spatial structure on the microscopic scale and is considered a continuous habitat. Still, a population with a self-imposed spatial structure emerged in our device due to the organization of cells into biofilms. Such emergent spatial population structures seem to be sufficient for the formation of selection amplifiers; however, in our case, they originate from endogenous dynamics of the population rather than the geometrical fragmentation implicit in the spatial structure of the habitat.

As opposed to a homogeneous culture (e.g., a stirred flask) with a global competition between cells/mutants, populations with spatial structure exhibit a more localized competition pattern. Emergent mutants contend mainly against their neighbors for resources, and their interactions with distant individuals are limited. Therefore, beneficial mutations at various locations may emerge, persist and avoid direct competition. This increases genetic diversity and reduces the effects of clonal interference, which may explain the relatively quick increase in resistance seen in our experiments.

In 48 hour samples, we found mutations in genes that are not related directly to the mechanism by which ciprofloxacin acts. Instead, these are stress response genes (parts of the *mar* and *sox* operons) are known to be important in general antibiotic and toxin resistance: they regulate the expression of efflux pumps and various surface structures (e.g., porins). Such mutations were also present in a sample in which cells experienced *on-chip* conditions but were not exposed to antibiotics (sample s1, s2), however, they demonstrated a 2-4× increase in MIC. Among the stress response genes, most frequently *marR* was affected, which is important in the regulation of the expression of the AcrAB efflux pump that plays a role in multidrug resistance. In one case (sample s6/2), we found a mutation in *acrR* itself, a direct regulator of *acrAB*. The pleiotropic nature of *marR*, *arcAB*, *rfa* and *omp* makes it possible that the microfluidic habitat induced mutations act as *exaptations* [Gould 1982]. In other words, they emerge due to the constricted environment, but later prove useful when cells adapt to high antibiotic regions in the channel. Our results suggest that exaptations may be most important in the early steps of evolutionary processes responsible for the emergence of resistance.

In a similar set of experiments, we studied the emergence of resistant *E. coli* bacteria in spatial concentration gradients of T4 bacteriophages [Nagy 2022b]. We saw the increase in phenotypic and genetic variability, as well as the emergence of phage-resistant mutants that spread across the microfluidic device. Genomic sequencing analysis showed that mutations primarily affected the receptor sites of the T4 phage in *E. coli* (OmpC, lipopolysaccharides), as well as some biofilm-related loci (*csg*, *rcs*).

Analysis of population fluctuations in structured environments

The structure of compound natural microbial habitats has a defining role in the maturation of microbial communities. Despite the recognition that landscape structure impacts metapopulation

dynamics, as of yet, no connection has been made explicitly between the physical properties of microbial ecological landscapes and their impact on metapopulations. Performing such an investigation requires precise control of physical properties defining the landscape in question. Emulating such complex physicochemical environments as a patchy microfluidic habitat landscape (Fig. 13A) we investigated the effect of changing the connectivity features of this landscape as *E. coli* forms a metapopulation [Wetherington 2022a]. We analyzed the spatial distributions of *E. coli* cells within the devices using Taylor's law, an empirical law in ecology which states that the variance in occupancy of a (meta-) population σ_φ^2 is related to the mean $\langle\varphi\rangle$ by a power law [Taylor 1961].

$$\sigma_\phi^2 = c\langle\phi\rangle^\alpha$$

Taylor's law, as a statistical phenomenon, has been observed far beyond the scope of ecology, present in cell biology, linguistics, social science, and even number theory in mathematics.
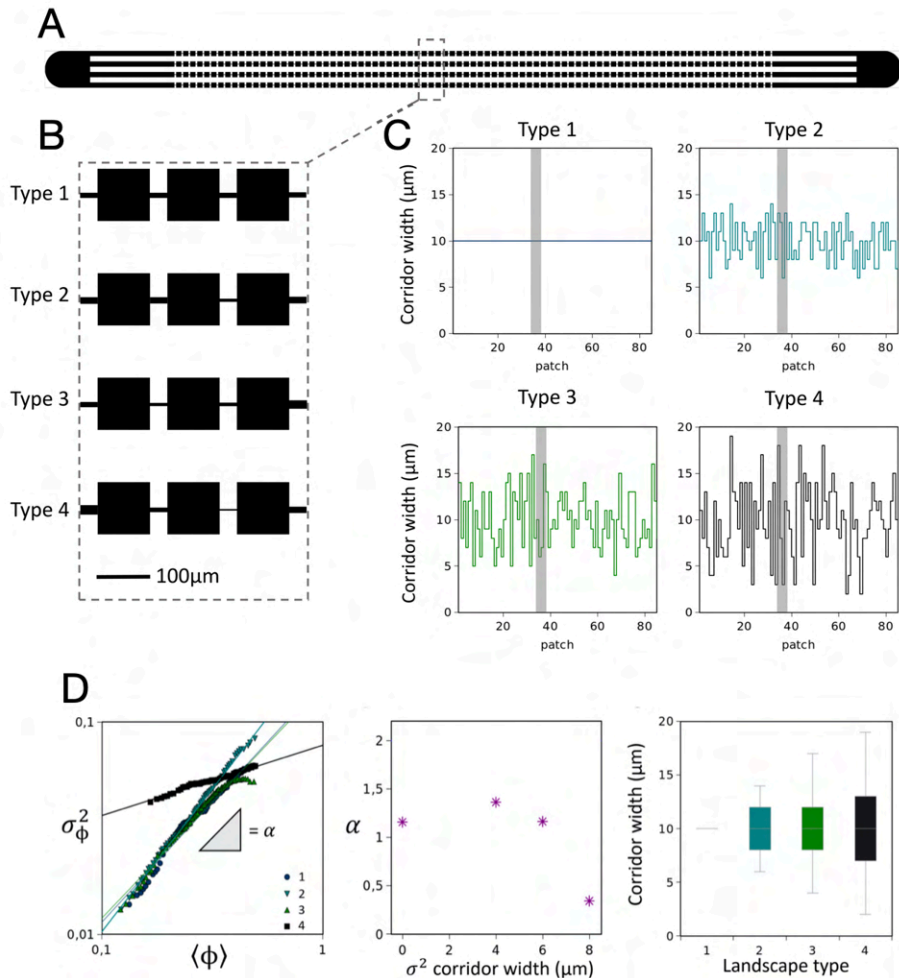
Figure 13. A) Schematic layout of the microfluidic device with single inlets on each side leading into 4 parallel habitat landscapes B) Zoom-in view of patch-corridor structure in each of the 4 parallel landscapes. For type 1 corridor width is kept constant at 10μm. For types 2-4 the average width is also 10μm thus, variance around the mean increases from type 1 to 4 as σ2 = 0, 4, 6, 8μm. This can be appreciated in C) where we show the pattern of corridor widths used for each landscape type. Grey shading indicates location of zoom-in on panel B. D) Left: the average occupancy of a patch, ⟨φ⟩, and its variance, σφ2 , in time. Lines represent the fit of the Taylor's law to the experimental data. Middle: the slope of the fitted Taylor's law, α, against the variance of corridor width. Right: a box plot of corridor widths around the mean (10μm).

We compared *E.coli* metapopulation distributions in different landscape types (Fig. 13AB). In order to achieve this, we studied the distribution of *E.coli* occupancy in microfluidic devices which consist of microscopic chambers (patches) connected by narrow channels (ecological corridors). Here, the only difference between landscape types was the within-landscape corridor width variance (Fig. 13BC) which we refer to as quenched disorder. Here we distinguish quenched disorder – which is exogenously imprinted into the ecological corridors as variance around the mean – from the time-dependent endogenous disorder constructed by local populations through microcolony and biofilm formation.

Starting from landscape type 1, which acts as our idealized "crystal-like" patchy habitat landscape, we steadily begin to increase quenched disorder in our landscapes, while maintaining a landscape average corridor width of 10 μm. After a relaxation time of 48 h after inoculation, images were captured from which patch occupancy can be deduced. In Fig. 13D we see that for landscape types 1-3, α values fall between 1.1-1.4. Strikingly, landscape type 4 does not follow suit, instead registering a value of $\alpha_4 \approx 0.34$, Fig. 3. These results suggest that beyond some critical level of quenched disorder (in this case (a corridor variance between 6-8 μm), a qualitative change occurs in the long-term distribution of *E.coli* metapopulations.

It remains to be seen exactly how these metapopulations arrive at this alternative statistical equilibrium. One possible explanation for these sharp transitions in metapopulation distribution is due to self-driven jamming by bacterial waves as they traverse the landscape. While speculative –as this research is ongoing– it would be an interesting contribution to the current field. This spatial ecology scenario with planktonic, free-swimming cell populations may parallel the dynamics of traffic jams.

Our results suggest that α is not only a trait of a species – originally asserted by Taylor – but likely a tunable characteristic that responds to external factors, or in this case – landscape properties.

Competition of *E. coli* and *P. aerugionosa* in structured environments

Maturation and ecological succession are terms that are often used interchangeably to describe some aspects of the dynamics of microbial communities. By expanding our focus to multi-species systems, we studied ecological succession in a bacterial meta-community of *E. coli* and *P. aeruginosa* in spatially distributed habitats structured at the micron-scale [Wetherington 2022b].

To imitate the patchy nature of microbial habitats, we used microfabrication to generate landscapes where arrays of habitat patches are connected by corridors. We fabricated 85 repetitions of a patch-corridor motif (Fig. 14A) giving rise to a one-dimensional crystal-like array of Micro Habitat Patches (MHPs). In these devices, we performed invasion-competition experiments using time-lapse microscopy of fluorescently labeled (red–green and green–red) co-cultures of strain pairs (*E. coli*– *P. aeruginosa*) to study ecological succession as the community develops over 48 hours.

We initiated the system with each species invading from opposite sides and recorded fluorescence microscopy images in 10 minute intervals. Local, within MHP occupancy was calculated for both *P. aeruginosa* and *E. coli* for all images. After initial colonization of the MHPs by *E. coli*, we see a clear pattern of ecological succession, where *P. aeruginosa* enters the habitat as a densely-packed front that advances and disperses through the patchy landscape. *P. aeruginosa* occupancy dynamics is considerably different from the fugitive dynamics of *E. coli* occupancy (Fig. 13B). As *P. aeruginosa* advances, *E. coli* retreats its range of high occupancy while keeping less localized and less dense fluctuating sub-populations. These local community dynamics (Fig. 13C) are observed repeatedly, following a classical ecological succession, where local species composition flows through the following states: (i) *E. coli* early colonization, (ii) expansion by recruitment, (iii) competition with invading *P. aeruginosa* and eventually (iv) replacement by *P.*
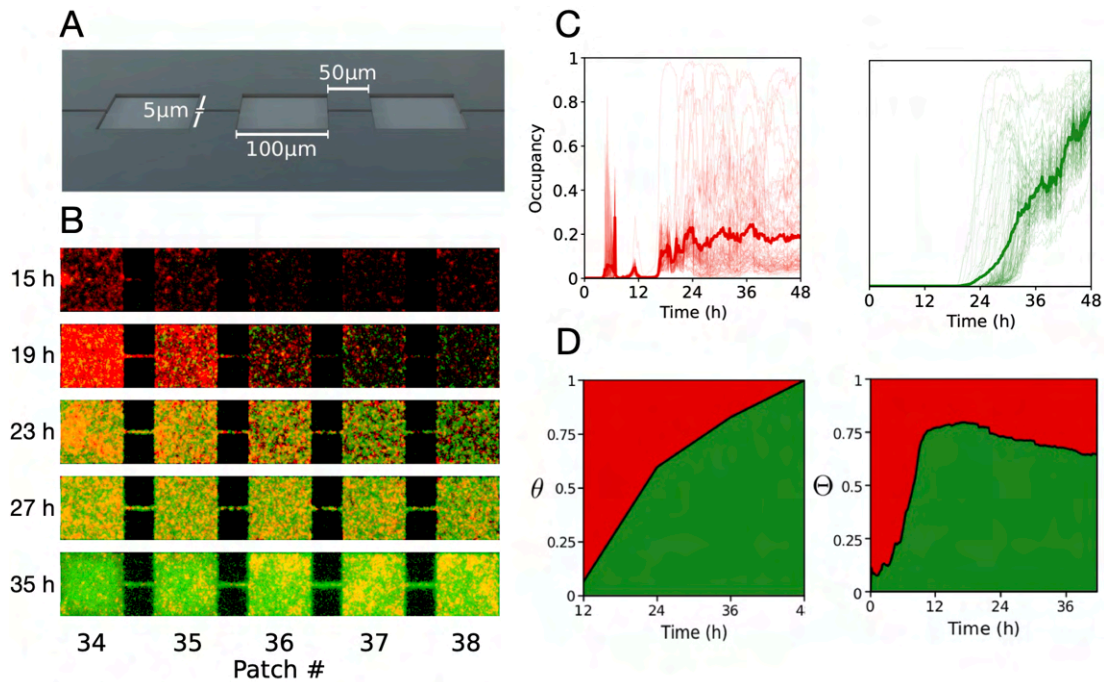
Figure 14. Competition colonization trade-off in micro-fabricated habitats. A) Scanning electron micrograph showing a section of a patchy landscape. B) Zoomed-in view of four patches at four different time points showing succession from *E. coli* (red) colonization to *P. aeruginosa* (green) invasion and dominance. C) Occupancy dynamics for *E. coli* (left) and *P. aeruginosa* (right) for all micro habitat patches in the array (light curves) and spatially averaged occupancy (thick curves). D) Left: community dynamics in well-mixed environments (stirred flasks) represented as *P. aeruginosa* fractional number occupancy, θ. Right: Metacommunity dynamics in patchy landscapes (microfluidic chip) represented as *P. aeruginosa* fractional spatial occupancy, Θ.

aeruginosa. Coexistence of alternative local community states can be observed even in adjacent patches as a consequence of stochasticity. In most experiments, however, there is remarkable determinism, which emerges as the statistical pattern in the temporal ordering of events of high occurrences. At multiple scales (from the single MHP level to the whole landscape) we see the heuristic pattern of ecological succession.

A mechanism for coexistence in patchy landscapes is habitat fragmentation by blockage of patch-corridor interfaces. These priority effects are responsible for holding back *P. aeruginosa* which in some cases ultimately can become fragmented, although often will eventually break through. Delaying *P. aeruginosa*'s arrival, *E. coli* increases its window of opportunity. The longer *E. coli* has free of competition, the more it increases its chances against *P. aeruginosa* and sometimes can dominate.

Our results demonstrate that *E. coli* is a fugitive species while *P. aeruginosa* is a superior competitor enacting a competition-colonization trade-off in patchy environments. Aggregation-dependent priority effects deterring competitor dispersal provide a mechanistic explanation for coexistence. These results highlight the importance of dispersal strategies in structuring and maturing microbiomes.

Closing remarks

During the time course of the project, we made substantial progress in achieving the proposed goals. Besides, we expanded the original concept and achieved new results in the area of microbial aging and community maturation.

We faced some difficulties during the experimental work, which took time to solve therefore our progress was slower than expected. Likewise, the pandemic posed some challenges that we had to face.

Altogether we prepared 7 article manuscripts during the project (2 published, 2 accepted, 3 under review). 2 manuscripts are under preparation, and more planned. One Ph.D. dissertation was written (acknowledging the OTKA grant) and successfully defended by Miles T. Wetherington (Pontificia Universidad Católica de Chile, Ph.D. in Biological Sciences) in 2021. Another dissertation is in preparation (Ágnes Ábrahám, University of Szeged, Doctoral School of Multidisciplinary Medical Sciences). We presented our results in numerous international and national conferences, both as talks and posters.

References

Ábrahám Á, **Buzás A**, Dér L, **Kelemen L**, **Nagy K**, **Galajda P**. Tracking and control of cell lineage in a microfluidic baby machine. (2022a) (manuscript in preparation)

Ábrahám Á, **Nagy K, Buzás A**, Csákvári E, Dér L, Pap I, **Kerényi Á**, **Galajda P**. Single-cell level quorum sensing response of *Pseudomonas aeruginosa* under dynamically changing conditions. (2022b) (submitted)

Bashir F, Kovács S, **Ábrahám Á**, **Nagy K**, Ayaydine F, Valkony-Kelemen I, Ferenc Gy, **Galajda P**, Tóth SzZ, Sass L, Kós P, Vass I, Szabó M. Viable protoplast formation of the coral endosymbiont alga *Symbiodinium* spp. in a microfluidics platform (2022) (submitted)

Beller L, Deboutte W, Falony G, Vieira-Silva S, Tito RY, Valles-Colomer M, Rymenans L, Jansen D, Van Espen L, Papadaki MI, Shi C, Yinda CK, Zeller M, Faust K, Van Ranst M, Raes J, Matthijnssens J. Successional Stages in Infant Gut Microbiota Maturation. *mBio* (2021) 12:e0185721

Nagy K, **Ábraham Á**, Keymer JE, **Galajda P.** Application of Microfluidics in Experimental Ecology: The Importance of Being Spatial. *Front Microbiol.* (2018) 9:p496

Nagy K, Dukic B, Hodula O, **Ábrahám Á**, Csákvári E, Dér L, Wetherington MT, Noorlag J, Keymer JE, **Galajda P**. Emergence of resistant *Escherichia coli* mutants in microfluidic on-chip antibiotic gradients *Front Microbiol.* (2022a) (accepted for publication)

Nagy K, Phan T, Bos J, **Galajda P**, Austin R. H.
Emergence of phage resistant bacteria in a microfabricated evolution accelerator (2022b), (manuscript in preparation)

Odum EP. The strategy of ecosystem development. *Science* (1969) 164:p262

Stewart EJ, Madden R, Paul G, Taddei F. Aging and death in an organism that reproduces by morphologically symmetric division. *PLoS Biol.* (2005) 3:e45.

Striednig B, Hilbi H. Bacterial quorum sensing and phenotypic heterogeneity: how the collective shapes the individual. *Trends Microbiol*. (2021) S0966-842X(21)00212-2.

Széles E, **Nagy K**, **Ábrahám Á**, Kovács S, Podmaniczki A, Nagy V, Kovács L, **Galajda P**, Tóth SzZ. Microfluidic Platforms Designed for Morphological and Photosynthetic Investigations of Chlamydomonas reinhardtii on a Single-Cell Level. *Cells* (2022) 11:p285 (2022)

Taylor LR. Aggregation, variance and the mean. *Nature* (1961) 189:p732

Tkadlec J, Pavlogiannis A, Chatterjee K, Nowak MA. Fast and strong amplifiers of natural selection. *Nat. Commun.* (2021) 12:4009

Wang P, Robert L, Pelletier J, Dang WL, Taddei F, Wright A, Jun S. Robust growth of *Escherichia coli. Curr Biol.* (2010) 20:1099-103.

Wetherington MT, **Nagy K**, Dér L, Noorlag J, **Galajda P**, Keymer JE. Quenched Disorder in Landscapes Leads to Shifts in Microbial Population Scaling. *Front Microbiol.* (2022a) (accepted for publication)

Wetherington MT, Dér L, **Nagy K**, **Ábrahám Á**, Noorlag J, **Galajda P**, Keymer JE. Ecological succession and the competition-colonization trade-off in microbial communities. (2022b), (submitted)

Wetherington, MT. The spatial ecology of microbes. PhD dissertation (2021)
https://repositorio.uc.cl/xmlui/handle/11534/59531 (acknowledging the OTKA grant)

Zhao Z, Fan R, Xu W, Kou Y, Wang Y, Ma X, Du Z. Single-cell dynamics of chromatin activity during cell lineage differentiation in Caenorhabditis elegans embryos. *Mol Syst Biol.* (2021) 17(4):e10075.